Contents lists available at ScienceDirect

Tunnelling and Underground Space Technology incorporating Trenchless Technology Research

journal homepage: www.elsevier.com

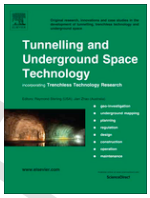

Thrust and torque components on mixed-face EPB drives

Claudia González,* Marcos Arroyo, Antonio Gens

Department of Geotechnical Engineering, Polytechnic University of Catalonia, Barcelona, Spain

ARTICLE INFO

Article history:
Received 9 October 2015
Accepted 13 January 2016
Available online xxx

Keywords:
EPB machine
Thrust
Torque
Cutting tool
Heterogeneous media
Soil

ABSTRACT

In this communication we propose a method to estimate net thrust and torque applied at the excavation front by cutting tools from EPB machines when they are working in mixed faces constituted by soils and soft rock. The method is inspired by similar simplifications used for the analysis of TBM drives in rock. The proposal is validated using a database of EPB registers which were gathered from more than 35 km of tunnel drives excavated in soils, soft rock and heterogeneous media. The results allow us to assess the influence of the type of ground excavated and its geotechnical properties on the net thrust and torque applied.

1. Introduction

Rational prediction of tool wear is highly dependent on accurate assessment of the loads applied by the cutting tools. This has been well appreciated since long for mechanized rock excavation in general and, in particular, for TBM design and performance evaluation (Bruland, 1998). For the case of EPB machines the situation is different. On the one hand the incorporation of face support complicates significantly the evaluation of tool loads. On the other hand the problem of face support is typically important in the conditions in which EPB machines operate. This means that it receives more attention than the issue of wear and its possible impact on machine performance, which may be seen as relatively unimportant. This vision is wrong, particularly if the EPB operates in mixed soil-rock terrains.

EPB field performance may be strongly affected by wear of the cutting tools and other elements of the machine. For instance, at the S-line metro do Porto the gross EPB advance rate was only 60% of that expected; the difference was mostly due to abrasiveness and tool wear (Nielsen et al., 2006). In the Seville Metro 1 line changes in EPB cutter head configuration, motivated by the excessive wear observed on site, lead to a doubling of gross advance rates (Lovat, 2000). Similar effects were noted also for the EPB machine working in the Deep Tunnel Sewerage System (DTSS) in Singapore (Zhao et al., 2007): wear motivated on site cutter-head modification was necessary to almost double gross advance rate (from 6 to 11 m/d).

It is difficult to individuate clearly what are the normal and tangential forces that act on EPB roadheader tools, because they are not separately recorded. EPB operational records usually include data on total applied thrust and supplied torque. Those signals include the contributions of other components such as face support, shield and chamber-wheel friction. The different components are machine-design dependent and generally known with very different degrees of certainty.

Thrust and torque component evaluations for EPB machines are performed at the design stage, so that torque and thrust capacities can be specified for machine commissioning (Melis, 2005; Lunardi et al., 2011). These evaluations are largely empirical and/or dependent on a number of general hypotheses about soil behavior and in situ conditions (initial stress state) of difficult verification. Moreover, since their overall purpose is machine dimensioning, safe upper bounds are favoured in the estimates. A conservative bias on such estimates might not be desirable for tool wear studies.

In this paper a different route is followed to estimate EPB tool loads. The aim is to develop a simplified method to exploit operational EPB data to evaluate average effective tool loads. In the next section we describe briefly design approaches currently used for thrust and torque component evaluation for EPB, commenting on their relation with operational data. Then we briefly describe the database of EPB drives whose data is examined. A methodology to extract tool load information from the operational data available in the database is described afterwards. Finally, we present some results obtained after the new methodology is applied to the database.

2. Background

2.1. Longitudinal equilibrium and thrust components

Thrust analysis for EPB machines is usually based on a quasi-static analysis of longitudinal machine equilibrium. This can be expressed as (Wittke, 2007)

$$F_p = F_n + F_s + F_F + \Delta F \tag{1}$$

where F_p is the total applied machine thrust, F_n is the normal force

* Corresponding author.
Email addresses: claudia.gonzalez@upc.edu (C. González); marcos.arroyo@upc.edu (M. Arroyo); antonio.gens@upc.edu (A. Gens)

http://dx.doi.org/10.1016/j.tust.2016.01.037
0886-7798/

on cutter tools. F_s is the resulting force supporting the ground/bentonite chamber, F_F is the frictional force between shield and ground and ΔF covers other loads such as back up friction.

a. *Total applied thrust*

Total applied thrust can be simply deduced as

$$F_p = \sum_i p_i A_i \tag{2}$$

where A_i is the cylinder section and p_i is the net hydraulic pressure applied at the cylinder. Cylinder pressure instrumentation data are typically recorded in EPB machines and F_p is therefore well determined in most drives.

b. *Normal thrust component due to the cutter tools*

Forces acting per tool are not usually measured during operation, so this component can be only indirectly verified.

For hard rock TBM design it is customary to estimate normal load per tool based on single or multiple rock-cutting experiments (see, for instance, Bilgin et al., 2012, and references therein). This approach is not easily adaptable for the geological conditions in which EPB typically operate (soft rocks, mixed soil-rock drives). To simplify, it is also generally assumed that all tools take the same normal load and therefore:

$$F_n = \sum_{i=1}^{n} f_{ni} = n f_n \tag{3}$$

where f_n is the normal load per tool and n is the number of tools in the cutterhead.

c. *Face support thrust component*

This force component is not present in open-face machines, but is essential for EPB machines. Formally it may be expressed as:

$$F_s = \int_A p_s dA \tag{4}$$

where A is the area of supported face excavation area and p_s is the applied support pressure. Face pressure needs to be maintained within certain limits to avoid collapse or blow-out. For soil-dominated conditions, these limits may be obtained at the design stage by means of limit equilibrium techniques (Anagnostou and Kovari, 1996), plastic analysis (Mollon et al., 2009) and/or numerical methods (Zhang et al., 2015). The later are also amenable to study more complicated cases such as mixed face rock conditions (Senent and Jimenez, 2015).

To enforce face pressure limits during operation chamber pressure measurements are used. These measurements provide therefore a direct means by which F_s can be accessed.

d. *Friction between shield and ground*

Formally, the friction load between shield and ground can be estimated as:

$$F_F = \int_{A_s} \mu \sigma_r dA \tag{5}$$

where μ is a friction coefficient and σ_r is the radial stress acting in the exterior shield surface, A_S. There is considerable uncertainty about both these quantities, particularly in soft rock and mixed face conditions. Radial stress depends on the original "in situ" stress state and in the details of the excavation process. Estimates based on the convergence confinement method have been proposed (Lunardi et al., 2011); other estimates may be also obtained from a 3D numerical simulation of the excavation process (Lambrughi et al., 2012). As for the friction coefficient, μ, estimated values range between 0.15 and 0.55 (Melis, 2005; Lunardi et al., 2011); values close to the lower end are usually assigned when lubricant sludges are employed. These lubricant sludges are injected through ports in the shield; injection pressure is monitored at these ports and that offers a close approximation to the acting radial stress. However, not all EPB machines have shield injection capabilities and, even when they have it, it is not always used.

A full scale test to estimate this component was presented by Gong et al. (2007). The EPB machine, with diameter 4.5 m, was excavating weathered granite. The pressured chamber was emptied and the shield was retracted from the excavation face. The force retracting the shield was the F_F component, which they quantified on average as 50 kN. Subsequently, a penetration test was performed at the same location, in which total thrust applied was 90–180 times larger than F_F.

e. *Other loads*

These include several components that are largely machine-dependent. For instance, (Melis, 2005), presents a computation in which two separate terms are included, the shield-lining friction and the back-up drag.

f. *Example result*

Lunardi et al. (2011) discuss the design of a large (D = 15.6 m) EPB for a tunnel on soft-rock conditions. Table 1 collects the proportions in which the different thrust components contribute to average and maximum applied thrust conditions (251 and 360 MN, respectively).

2.2. Rotational equilibrium and torque components

A first approximation to the rotational equilibrium of an EPB machine can be written as (Wittke, 2007):

$$M_p = M_C + M_S + \Delta M \tag{6}$$

where M_P is the torque supplied to the front wheel, M_C is the torque due to cutting and excavation by tools mounted on the front wheel, M_S is the torque due to the friction against the cutterhead and ΔM involves other components (e.g. friction at the wheel perimeter). As for the case of thrust, the different torque reaction components are estimated with more or less approximation for design purposes. These estimations are not often verified in detail during construction.

a. *Torque supplied*

Table 1
Components of the total Thrust E and represented percentage (Lunardi et al., 2011).

Load	% *E*	% *E max*
Fn	8	6
Fs	30	42
ΔF	4	3
F_F	58	50

Power, P_e, supplied to the various engines driving the wheel is generally recorded during EPB operation. Also the angular speed of the wheel, ω is typically recorded during operation. If overall engine efficiency, e, is also known, torque supplied can then be obtained as

$$M_p = e\frac{P}{\omega}$$

In most EPB machines torque supplied is computed and recorded automatically during operation. Note that torque supplied to the front wheel must be balanced by another equal and opposed torque. In an EPB machine this reaction torque results mostly from shield friction with the surrounding ground, although the thrust pistons may also contribute some tangential component.

b. *Torque due to tool actions*

Formally, the torque due to front-wheel tool actions can be expressed as:

$$M_C = \sum_{i=1}^{n}(f_{ri}r_i) = \sum_{i=1}^{n}(C_{ci}f_{ni}r_i) \quad (7)$$

where f_{ri} is the tangential force acting on tool i, r_i is the distance from that tool to the rotation axis, C_{ci} is a cutting coefficient i. A simplified version results if all normal forces and cutting coefficients are assumed equal.

$$M_C = C_c f_n \sum_{i=1}^{n} r_i \quad (8)$$

For rock cutting discs mounted on TBM, individual cutting coefficients are obtained through dedicated linear cutting tests (LCT) or estimated from semi-empirical formulas such as, (Hughes, 1986)

$$C_c = 0.65\sqrt{\frac{2Prev}{d}} \quad (9)$$

where d is the cutter disc diameter and p_{rev} is penetration per revolution. A similar approach is used for picks. For soils and soft rocks the approaches to evaluate cutting coefficients or tangential forces are less well-established, and several hypothesis based on passive failure are used (Melis, 2005).

c. *Torque due to friction against the wheel*

According to Wittke (Wittke, 2007) M_S is obtained as:

$$M_s = \xi M_E \quad (10)$$

where ξ is the factor that takes into account the contribution of the excavated ground inside the cutterhead, M_E is the resistant torque caused by the ground in front of the excavations, defined as the area integral of the circumferential tangential stress in the frontal bulkhead.

$$M_E = \int_A r\tau dA \quad (11)$$

To estimate this stress a constitutive model for the material in contact with the bulhead is necessary. Wittke (2007) describes two hypothesis, one in which a non-Newtonian Bingham fluid model is used, another in which a plastic flow criteria described by a Mohr-Coulomb envelope is applied. For this later case

$$\tau = p_s \tan\varphi + c \quad (12)$$

where p_s is the instantaneous face support pressure, φ and c are the relevant values of friction and cohesion. Whatever the constitutive model there may be considerable uncertainty about the relevant parameters, due to unclear drainage conditions for the cutting process, the effect of remoulding and mixing on ground properties, the effect of additives, etc.

d. *Example*

Melis (2005) explains the torque capacity design estimates made, along the lines just described, for a large EPB commissioned for the M30 project in Madrid (Melis, 2005). The torque components estimates are summarized in Table 2. The friction term clearly overwhelms the other contributions (see Table 3).

3. Database description

3.1. Tunnel drives and EPB characteristics

During the last 15 years major changes in the mass transit systems within the metropolitan area of Barcelona resulted in the execution of several tunnels. Two of the main projects were the metropolitan Line 9 ("Linea 9") and the Terrassa Railways extension. These two projects included the 11 tunnel drives considered here, with a total tunnel length of above 33 km. Line 9 tunnels were designed for two tracks and have relatively large diameters. Their main characteristics are summarized in Table 1, where Line 9 tunnel drives are labelled UP. More details about the different tunnel drives can be found in González, C., (2014).

The main features of the 5 TBM-EPB employed in these drives are summarized in Table 4. Most EPB (4) machines were used in more than one drive, sometimes after retooling. Except for the case of

Table 2
Torque components estimate for a large EPB in soft rock (Melis, 2005).

Component	(% *Mp*)
Mc	0.5
Ms	98.7
ΔM	0.87

Table 3
Tunnel drives: main characteristics.

Drive	Contract name	Length [m]	Diameter [m]
UP1	IV A Can Zam	4293	11.95
UP2	IV B Gorg	4000	11.95
UP3	IV C Trajana	645	11.95
UP4	IV C Doble tunnel	1300	11.95
UP5	IV D Doble tunnel	1508	11.95
UP6	II Bif.- Z. Univ.	3310	11.95
UP7	IA Eixample N-Entre pistas	4328	9.4
UP8	IB Fira II-Parc Logistic	1065	9.4
UP9	IC Eixample N-Parc Logistic	6687	9.4
EI	Egara I	3147	6.9
EII	Egara II	3132	6.9

Table 4
TBM-EPB features.

Perforation units (UP)	2/5	1/3/4	6	7/8/9	EI and EII
Manufacturer[a] [–]	HN	NFM-W	HN	HN	L
Diameter	12	12	12	9.4	6.7
Shield length [m]	12.6	12.6	11.3	10	8.9
Cutter head rotational velocity [rpm]	0/2.6	0/3.7	0/2.6	0/3.2	0/3
Installed power [MW]	6.2	7.3	4	6	2.8
Cutterhead nominal torque [MN m]	38	28.9	38	22.6	9.6
Cutterhead exceptional torque [MN m]	45.6	37	45.6	26.4	12.7
Thrust cylinders [–]	38	30	38	26	26
Total nominal thrust [MN]	110	90	121	85	65
Total exceptional thrust [MN]	138	110	138	106	80.3
Nominal and max. EPB pressure [MPa]	0.45	0.3	0.45	0.4	0.4
Minimum turning radius [m]	270	270	300	250	160
% opening [%]	33	26	33	31,4	32,8
Number of tools	322	83/352/358	322	322	160
Number of discs	42	83/66/72	42	42	0
Number of picks	264	0/238/238	264	264	56
Number of scrapers	16	0/48/48	16	16	104

[a] Herrenknecht (HN), Wirth (W), Lovat (L).

UP1, where the only tools mounted were discs, the cutter head configurations included a variable number of discs, picks and scrapers, also indicated in the table. More details about these machines can be found in González et al. (2014).

3.2. Geotechnical conditions

The Barcelona hinterland is quite varied from the geotechnical viewpoint. Topographically is marked by a mountain range running broadly parallel to the seafront. Between these two barriers alternate a number of smaller hill chains and valleys. Two of these valleys are occupied by relatively larger rivers that end in deltas. A Paleozoic basement, where granodiorite intrusive rock dominates, is found at varying degrees of weathering throughout the city. This batholith is frequently intruded by porphyry dikes. Basement rocks also include Cambro ordovisian cornubianites. Over that basement tertiary Miocene and Pliocene coarse and fine grained materials occupy large areas, Pleistocene clayey soils are more frequent as the sea approaches. Thick Quaternary deposits appear in the vicinity of the two main rivers Llobregat and Besos, with a variety of depositional environments and coarse/fine material distributions.

The different geotechnical units encountered in the tunnel drives are listed in Table 5; the mean value of some of their geotechnical properties like unconfined compressive strength (UCS) and LCPC abrasivity value is also given. More details about the different units and the LCPC abrasivity measurements may be found in González et al. (2014) and González (2015). The geotechnical units intercepted in each tunnel drive are also defined in Table 5.

A characteristic of the database under study was noticeable material heterogeneity in both the longitudinal and transverse section. A geotechnical stretch, TG, is defined as one in which materials at the mixed face maintain, approximately, a constant areal proportion and spatial disposition. A large population of TG was obtained after identifying all the TG appearing alongside each drive. Then geotechnical properties were assigned to each one as weighted averages of those of the geotechnical units appearing at the tunnel face. The resulting statistics (mean and coefficient of variation, CV) for UCS and LCPC abrasivity of geotechnical stretches, broken down by tunnel drive, are presented in Table 6. The process is described in detail in González et al. (2015), where more data can be found about the longitudinal and transversal geotechnical variability of these tunnels.

Examining Tables 5 and 6 it may be noted that UP7, 8 and 9 perforated mostly soft soils, UP1 perforated mostly rocks and the others a variety of hard soils and soft rocks (see Fig. 1).

Table 5
Geotechnical Units (GU) in the database.

Name	Type	Acronym	UCS (Mpa)	Abr (g/t)	Present in drive
Paleozoic					
Granodiorite	Strong rock	Gr1(II)	95	1080	1/2/3/5
	M. strong rock	Gr1(III)	26.3	400	1/2/3/4/5/6
Granite weathering	Stiff soil coarse/weak rock	Gr2(III–IV)	0.28	880	1/2/3/4/5/6
	Firm soil coarse	Gr2(V)	1.2	778	1/2/3/4/5/6
Granite weathering	Weak rock/ stiff soil coarse	Gr2(IV)	0.1	320	1/2/3/4/5/6
Porphyd	Strong rock	Pf	97	780	1
Granodiorite Cambro-Ordovisic	M. strong rock	Bf + Gr2 + CO	14.7	440	1
Cornubianite	M. strong rock	Co	32.5	398	1
Cambro-Ordovisic-Siluric-Devonic	Weak rock	Spv + Dc + CO	1.95	920	6
Limestone	M. strong rock	Dc	43	758	6
Tertiary					
Tertiary miocene	M. strong rock	M1	12.6	1077	1/2/3
Tertiary miocene	Very stiff s. coh.	Ma	0.21	399	EI/EII
Tertiary miocene	Very stiff s. coar.	M/Mg	0.42	498	6/EI/EII
Pliocene	Very stiff s. coh.	Pl1	0.34	738	2/3/4/5/6
		Pl2	0.4	20	2/3/4/5/6
Quaternary					
Pleistocene ancient	Very stiff s. coh.	Qa	0.35	40	2/3/4/5
Pleistocene Tricicle	Firm soil coarse	Qcb/Qcs	0.12	461	2/3/4
Quaternary holocene Besòs delta				957	2/3/4
	Qb4		0.09	280	2/3/4
	Qb3/Qb3s		0.08	80	2/3/4
	Very soft s. coar.	Qb2/Qb2g	0.04	35	2/3/4
	Soft soil coarse	Qb1	0.19	10	2/3/4
Quaternary alluvial	Soft soil coarse	Qrg	0.07	40	2/3
	Stiff soil coarse	Qr	0.24	60	2/3
Quaternary Pleistoc.	Firm soil coarse	PQ	0.13	120	2/3/4/5
Quaternary Holocene LLobregat	Soft soil coarse	Ql3/Ql3s	0.06	320	7/8/9
	Very soft s. coar.	Ql2/Ql2g	0.016	180	7/8/9
Quaternary cohesive				399	7/8/9
Quaternary coarse	Stiff soil coh.	Qc	0.17	400 199.6	2/3/4 EI/EII
	Stiff soil coarse	Qg	0.15	200.4	EI/EII

Table 6
TG geotechnical property statistics broken down by tunnel drive.

Drive	N[TG]	UCS[TG] (MPa)	CV (RCSeq[TG])	Abreq[TG] (g/t)	CV (Abreq[TG])
1	35	61.4	0.31	734.5	0.26
2	23	7.4	3.01	545.9	0.45
3	14	0.24	0.31	356.9	0.38
4	12	0.34	0.57	306.7	0.68
5	21	3.1	2.33	422.6	0.37
6	4	12.7	0.73	164.9	0.72
7	6	0.03	0.38	28.6	0.50
8	3	0.02	0.44	18.7	0.81
9	25	0.03	0.47	23.0	0.79
EI	20	0.3	0.39	298.7	0.30
EII	20	0.3	0.39	298.7	0.30

3.3. Production and performance data

Based on production records and site information the gross advance rates Ar for each drive are presented in Table 7. Production curves for the different L9 drives are also represented in Fig. 5 as chainage vs time. With gross advance rate values Ar and net advance rate PR the U coefficient is determined in each UP drive (Table 7). It is striking the small U value observed for UP2. This was a result of layout modifications with respect to the original project. A forced stoppage of 9 months approximately ensued, which disrupted significantly the gross advance rate Ar (see Fig. 5). The value Tr in Table 7 indicates the estimated amount of the total tunneling time that was employed in repairs and maintenance of the cutting wheel. More details about time breakdowns for each project can be found in González et al. (2014).

The machines usually record the operational data every 3 min. There were some gaps in the records (Table 8), but still the total collected data rise to $4.1 \cdot 10^{10}$ items. For this work only 13 operational parameters were selected (thrust (E), Torque (PM), gross advance rate (Ar), net advance rate (PR), penetration rate (Prev), rotational velocity of the cutterhead (VRDC), chamber pressure records (6 channels) and, where available, shield injection pressure. The original data were averaged to obtain a representative mean value for each lining segment rings. Even after this averaging the database included 17,293 records.

4. Simplified thrust and torque analysis for EPB drives

4.1. Thrust component estimation

As explained above, some components of the thrust equilibrium equation are difficult to relate with the recorded data, so a simplified version is used

$$F_p = \lambda_{EPB}(F_n + F_s) \tag{13}$$

where we introduce λ_{EPB}, the thrust amplification factor, taking into account the hard to measure components F_r and ΔF. An analogous equation has been employed (Rostami and Ozdemir, 1993) for rock drives

$$F_p = \lambda_{TBM} F_n \tag{14}$$

From the simplified equilibrium equation it follows that

$$\frac{(F_r + \Delta F)}{F_p} = 1 - \frac{1}{\lambda_{EPB}} \tag{15}$$

4.2. Torque component estimation

Similarly, the rotational equilibrium equation for the EPB is simplified introducing a torque amplification factor, κ_{EPB}

$$M_p = \kappa_{EPB} M_c \tag{16}$$

The implication is that

$$\frac{\kappa_{EPB} - 1}{\kappa_{EPB}} = \frac{M_S + \Delta M}{M_p} \tag{17}$$

However we do not have any direct data on $M_S + \Delta M$ with which to estimate κ_{EPB}. A different approach is needed.

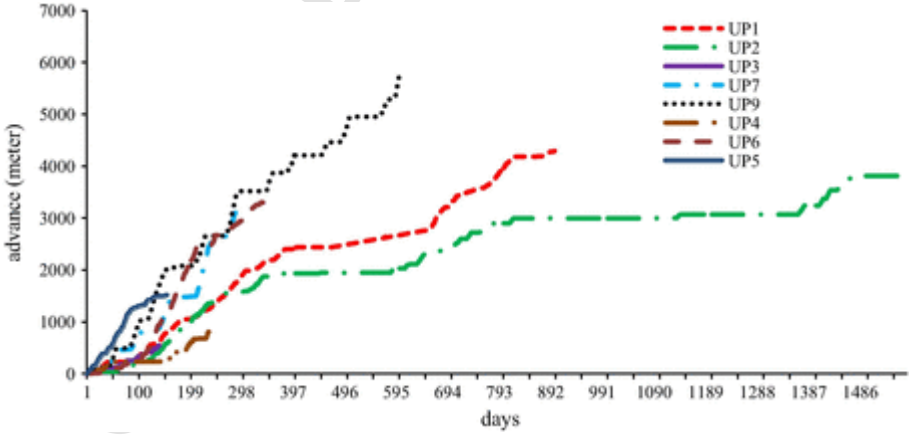

Fig. 1. Production curves for L9 tunnel drives.

Table 7
Production parameters of each tunnel drive in the database.

UP	Duration [days]	PR [m/day]	Ar [m/day]	U = Ar/PR [%]	Tr [%]
1	900	50	4.8	9	14
2	1470	104	1.7	2	12
3	120	43	4.5	11	26
4	270	60	4.8	9	46
5	180	52	8.4	16	30
6	390	67	8.5	13	19
7	330	79	9.4	12	4
9	182	81	9.7	12	4
E I	690	109	8.1	7.4	–
E II	390	115	8.4	7.2	–

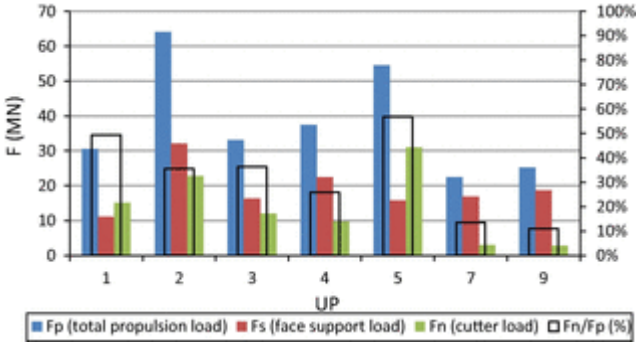

Fig. 2. Average thrust component decomposition for the different L9 drives.

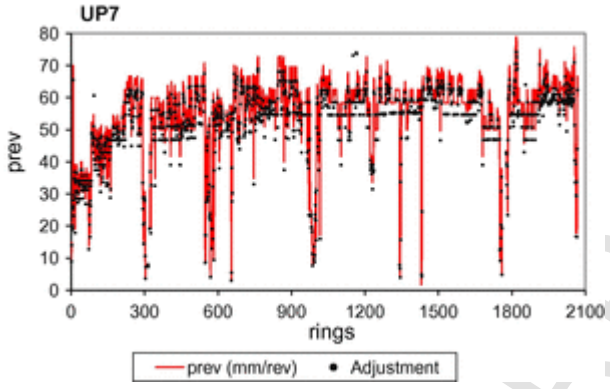

Fig. 3. Measured and adjusted values of penetration rate in UP7 drive.

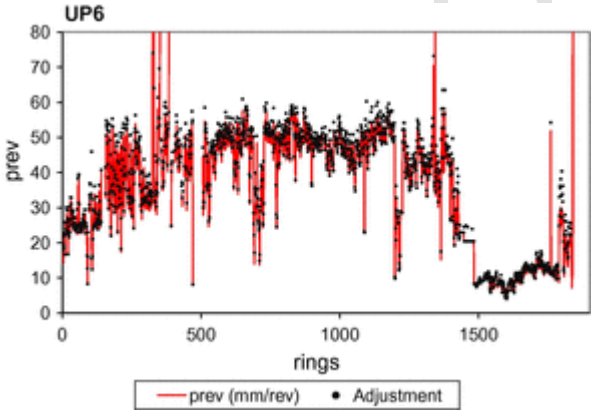

Fig. 4. Measured and adjusted values of penetration rate in UP4 drive.

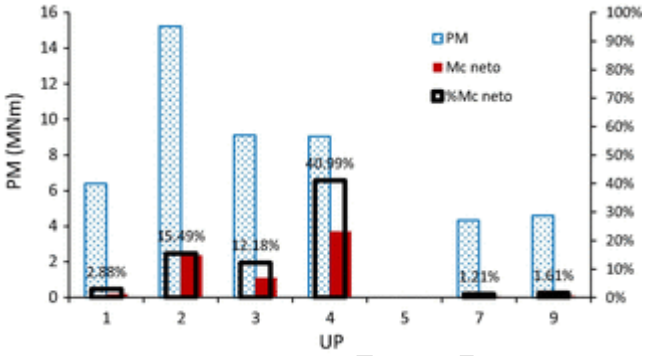

Fig. 5. Torque decomposition estimates.

Table 8
Data availability for the different drives.

Drive	Production	Maintenance (%)	Operation
UP1	100%	100	99.5%
UP2	100%	49.3	49.3%
UP3	100%	100	100%
UP4	100%	100	78.1%
UP5	11.6%	100	49%
UP6	100%	100	100%
UP7	100%	100	100%
UP8	NA	100	NA
UP9	86%	100	100%
EI	1.7%	74	74%
EII	1.4	81	81%

In rock TBM studies (Rostami et al., 1994) the following relation is applied to estimate cutting moment

$$M_c = f_r \bar{r} n \tag{18}$$

where n is number of tools, $\bar{r}$ is average tool radius and f_r is tool rolling force –assumed equal for all tools. If it is further assumed that all tools have the same unit normal and circumferential forces, the cutting coefficient can be related to machine-related quantities

$$C_c = \frac{f_r}{f_n} = \frac{M_c}{\bar{r} F_n} = \frac{\lambda_{EPB}}{\kappa_{EPB}} \frac{M_d}{\bar{r} F_p} \tag{19}$$

As stated before, relations between tool penetration depth p and cutting coefficient, C_c are available from experimental rock cutting studies. One such relation is that of Roxborough and Phillips (1975)

$$C_c = \frac{f_r}{f_n} = \sqrt{\frac{p}{d-p}} \tag{20}$$

where f_n is normal force on the tool and d is the disc diameter. This equation, which was developed for single discs, is adopted as model to propose an analogous expression for the whole EPB machine. We have then

$$C_c = \sqrt{\frac{p_{rev}}{\alpha D - p_{rev}}} \tag{21}$$

where p_{rev} stands for penetration per revolution, an available measure of machine performance, D is the EPB diameter and α is a newly introduced fitting parameter.

Combining now (18) and (21) it appears that

$$\frac{\lambda_{EPB}}{\kappa_{EPB}}\frac{M_d}{\bar{r}F_p} = \sqrt{\frac{p_{rev}}{\alpha D - p_{rev}}} \tag{22}$$

which can be further manipulated to obtain

$$p_{rev} = \frac{\alpha D}{\left(1 + \frac{\lambda_{EPB}}{\kappa_{EPB}}\frac{M_d}{\bar{r}F_p}\right)^2} \tag{23}$$

This equation may be used to exploit the construction records to obtain values for the unknown parameters, α, κ_{EPB}, λ_{EPB}. How best to proceed may depend both on the extent and contents of the database analyzed.

5. Application

5.1. Estimation of the thrust amplification factor

Ideally, full scale friction tests such as those described by Gong et al. (2007) should be employed to evaluate λ_{EPB}. In their absence shield injection pressure records may be used. We had data on shield bentonite injection pressure on a stretch of 164 lining rings of the *UP2* tunnel drive, traversing mixed faces with Pliocene (*Pl1* and *Pl2*) and Quaternary (*Qr* and *Qb*) geotechnical units.

Following Lunardi et al. (2011) we assumed a shield-ground friction value $\mu = 0.15$ and that other loads (ΔF) represented 3% of applied thrust. From the recorded machine data average values of F_p and F_s were obtained. On this basis a thrust component decomposition was performed as explained in Table 9.

Substituting the relevant values in Eq. (15) above it turns out that the thrust amplification factor λ_{EPB} is 1.2. Interestingly, the same value is typically used for λ_{TBM} (Rostami and Ozdemir, 1993). It was therefore assumed that $\lambda_{EPB} \approx 1.2$ could be taken as a good approximation for all the database.

5.2. Evaluation of applied thrust components

The normal thrust component may be then evaluated as

$$F_n = \frac{F_p}{\lambda_{EPB}} - F_s \tag{24}$$

Table 9
Thrust load components for rings 1825–1989 of UP2.

F_i	Value (kN)	Formulation	F_i/F_p (%)	Comments
F_p	56,000		100	Recorded
F_s	25,760	$P_s \pi r^2$	46	P_s = 2.48 bars average chamber pressure
F_F	7734	$\mu P_b \pi D_{ext} L$	14	P_b = 1.08 bars average shield pressure μ = 0.15. D_{ext} = 12.06 m, L = 12.6 m
ΔF	1680		3	Assumed
F_n	20,827	$E - (F_s + F_F + \Delta F)$	37	

This evaluation can be made at different levels of detail, from a single ring to the whole database. Here we have separately evaluated average values for each tunnel drive. The results are shown in Fig. 2. In general, in drives where more rock is present along the drive (case of *UP1* and *UP5*) *Fn* is proportionally larger, whereas in *UP* where soils are prevailing the situation is inverse, especially in the *UP7* and *9* where very soft soils are excavated and most thrust is applied to support the face F_s leaving less than 10% to F_n. It is also interesting to note how the EPB was pushing harder on drive UP2, which attained the fastest net advance rates (and, because of the aforementioned stoppages, the lowest gross advance rates).

5.3. Evaluation of applied torque components

To obtain a torque decomposition Eq. (23) is applied. All quantities are known except α and κ_{EPB}. Production records for M_d, F_p and p_{rev}, averaged at the single ring scale, were used to adjust a single value for α and a drive-dependent set of values for κ_{EPB}. The adjustment was made by trial and error, with the constraint that all κ_{EPB} values had to be greater than 1. An example of the fit obtained after adjustment is given in Figs. 3 and 4.

The value adjusted for α was 0.15. The drive-dependent torque amplification factor values have been used to obtain the torque decomposition illustrated in Fig. 5. In *UP5* the records of supplied torque were missing and the method could not be applied. For the UP1 drive only the rings in which the machine operated in closed EPB mode were analyzed.

Because the stronger rock stretches of UP1 have been excluded from the analysis, the harder terrains are those in UP2 to UP4, resulting in larger torque component due to tool action. It is noted that UP4 was also the drive in which a larger fraction of time was spent in tool maintenance. In the soft soil cases the M_c torque is less than 2% of total. Although these results are close to the estimates published by Melis for the M30 case, it is noted that the material excavated there was a soft rock, perhaps more analogous to other drives in the database.

6. Conclusions

In this paper a methodology to estimate the components of thrust and torque due to tool ground interaction from EPB production records has been presented and applied to a database of Barcelona tunnels. The estimates obtained are in line with "a priori" values obtained in other projects, but seem more sensitive to geotechnical conditions. Because the database comprises a variety of terrains ranging from rock to soft soil the effect of geotechnical conditions on the relative importance of thrust and torque components can be assessed. The relation of the estimated load decomposition with the tool consumption observed in these projects will be the subject of further research.

7. Uncited references

.

References

Anagnostou, G., Kovari, K., 1996. Face stability conditions with earth-pressure-balanced shields. Tunn. Undergr. Space Technol. 11 (2), 165–173.

.

Bilgin, N. e. a., 2012. Effect of replacing disc cutters with chisel tools on performance of a TBM in difficult ground conditions. *Tunnelling and Underground Space Technology,* pp. 41-51.Bruland, A., 1998. Hard Rock Tunnel Boring. PhD thesis

Norwegian University of Sciences and Technology of Trondheim (NTNU), Trondheim.

Gong, Q., Zhao, J. & Jiang, Y., 2007. In situ TBM penetration test and rock mass boreability analysis in hard rock tunnels. *Tunnelling an Underground Space Technology,22(3)* pp. 303-316.González, C., 2014. Performance, Wear and Abrasiveness in Mechanized Excavation of Tunnels in Heterogeneous Media. PhD Thesis Universitat Politecnica de Catalunya, Barcelona. p. 529 (in Spanish).

González, C., Arroyo, M., Gens, A., 2014. Abrasivity Measures on Geotechnical Materials of the Barcelona Area. In: Eurock2014. Vigo, España. .

González, C., Arroyo, M., Gens, A., 2015. Wear and abrasivity: observations from EPB drives in mixed soft – rock sections. In: Geomechanics and Tunnelling. vol. 8. Ernst & Sohn Verlag für Architektur und technische Wissenschaften GmbH & Co. KG, Berlin, pp. 258–264. N° 3.

Hughes, 1986. The Relative Cuttability of coal measures rock.. *Min. Sci. Techn. 3,* pp. 95-109.Lambrughi, A., Rodríguez, L.M., Castellanza, R., 2012. Development and validation of a 3D numerical model for TBM–EPB mechanised excavations. Comput. Geotech. 40, 97–113.

Lovat Inc., 2000. TBM Design Metro Seville Line 1: Solutions to Difficult Conditions . http://www.lovat.com/pdfs_powerpoints/Articles-&-papers..

Lunardi, P., Gatti, M., Cassani, G., 2011. The largest TBM-EPB machine in the world, designed to the Appennines. The experience of the Sparvo Tunnel. In: 1° Int. Congress on tunnels and underground structures in South-East Europe. Using Underground Space. Dubrovnik. Croatia. .

Melis, M., 2005. Las Tuneladoras de 3 carriles de la M-30. Revista de obras Públicas (ROP) 71–106.

Mollon, G., Dias, D., Soubra, A.H., 2009. Face stability analysis of circular tunnels driven by a pressurized shield. J. Geotech. Geoenviron. Eng. 136 (1), 215–229.

Nielsen, B., Dahl, F., Holzhäuser, J., 2006. Abrasivity of soils in TBM tunneling. Tunnels Tunnelling Int. 36–38.

Rostami, J., Ozdemir, L., 1993. A new model for performance prediction of hard rock TBMs. In: En: RETC Proceedings Conference. Boston, MA. USA. , pp. 793–809 (Chapter 50).

Rostami, J., Ozdemir, L., Neil, D., 1994. Application of heavy duty roadheaders for underground development of the yucca mountain exploratory study facility. In: Proc. Int. High Level Radioactive Waste Management Conference HLRWM. Las Vegas, Nevada. pp. 22–26.

Roxborough, F.F., Phillips, H., 1975. Rock excavation by disc cutter. Int. J. Rock Mech. Min. Sci. Geomech. Abs. 361.

Senent, S., Jimenez, R., 2015. A tunnel face failure mechanism for layered ground, considering the possibility of partial collapse. Tunn. Undergr. Space Technol. 47, 182–192.

Wittke, W., 2007. Methods of mechanized tunneling. (WBI), ed. Geotechnical Engineering in Research and Practice. Aachen: Statik und Konstruktion maschineller Tunnelvortriebe. Geotechnik in Forschung und Praxis, WBI-PRINT 6, VGE-Verlag Glückauf GmbH, Essen 2006, ISBN 978-3-7739-1306-7. Zhao, J., Gong, Q., Eisensten, Z., 2007. Tunnelling through a frequently changing and mixed ground: a case history in Singapore. Tunn. Undergr. Space Technol. 22, 388–400.

Zhang, C., Han, K., Zhang, D., 2015. Face stability analysis of shallow circular tunnels in cohesive–frictional soils. Tunn. Undergr. Space Technol. 50, 345–357.